Space-Variant Smoothing in Median-Regularized Reconstruction for Transmission Tomography

Ji Eun Jung[1,2] **and Soo-Jin Lee**[1,*]
[1]*Department of Electronic Engineering, Paichai University; Daejeon, Republic of Korea*
[2]*Department of Computer Science and Electrical Engineering, Kumamoto University; Kumamoto, Japan*
[*] *sjlee@pcu.ac.kr*

Abstract

We present a penalized-likelihood (PL) reconstruction method for transmission tomography where a new type of regularization, namely the weighted median regularization, is used in place of the conventional local smoothing-based regularization. In this work we note that, since the performance of the weighted median regularization is affected by the smoothing parameter that weights the regularization term with respect to the likelihood term, it is challenging to choose an optimal value of the parameter. To overcome this problem, we propose an adaptive method of choosing the smoothing parameter based on the pixel roughness derived from the histogram of a point-wise standard deviation image at each PL iteration. Our experimental results show that the proposed method provides acceptably good reconstructions which are almost comparable to the best reconstructions obtained with manually chosen smoothing parameter.

Introduction

With the rapidly growing use of transmission tomography, such as X-ray computed tomography (CT), efforts have been made to minimize radiation exposures by using model-based iterative reconstruction (MBIR) methods. [1] However, most of the MBIR methods use the penalty functions initially developed for emission tomography reconstruction, where the penalty function was designed to reflect the spatial characteristics of the underlying source distribution. However, the fundamental differences between transmission and emission scans require different approach to designing the penalty function. In fact, transmission tomography usually shows relatively sharp anatomical boundaries compared to emission tomography, which is due to the fact that different tissues and organs have different photon attenuations.

Recently, we have introduced the weighted convex median prior [2], [3] (in the context of a maximum *a posteriori* approach) that can efficiently preserve the fine details by adaptively choosing the center weight for the median. However, the performance of the algorithm using the adaptive weighted median prior (WMP) [3] turned out to rely on the smoothing parameter that weights the penalty term with respect to the likelihood term. This is due partly to the functional similarity between the center weight of the WMP and the smoothing parameter. Increasing the center weight of the median prior has an effect of better preserving the fine details but also has an unfortunate effect of increasing noise because the corrupted center pixel becomes less probable to be changed due to the larger center weight. [4]-[8] This behavior is similar to decreasing the smoothing parameter in conventional penalized-likelihood (PL) reconstruction. Therefore, it is important to study how to determine the smoothing parameter so that the image reconstructed by the PL-WMP method remains as accurate as possible.

In this work we develop an adaptive method of choosing the smoothing parameter for PL-WMP reconstruction. More precisely, the purpose of this work is to develop a space-variant smoothing method for a given center weight of the WMP. Here we assume that the center weight for the median is properly chosen and search for an optimal value of the smoothing parameter at each pixel location by using the information on the roughness of the neighbor. The technical challenge in this case is to investigate how to make the smoothing parameter be adaptively chosen so that the WMP does not degrade the reconstruction when the center weight is relatively high.

The final goal of our work would be to combine the adaptive WMP reported in [3] with an adaptive method of choosing the smoothing parameter, which will be proposed in this work, so that both of the two closely-related parameters can be adaptively chosen. In this work, however, we restrict ourselves to the case where the weight for the median prior is fixed over the entire reconstruction process.

This work is organized as follows. In the Method section, we introduce a space-variant smoothing method for PL-WMP reconstruction followed by an optimization algorithm that can approximately maximize the overall objective function for our proposed method. In the Experimental Results section, we present and discuss the experimental results obtained from our simulation studies using a software phantom. Finally, we draw our conclusions.

Space-Variant Smoothing for PL-WMP

PL reconstruction in transmission tomography is to seek the attenuation coefficients $\mathbf{\mu}$ of an underlying object by the following minimization:

$$\hat{\mathbf{\mu}} = \arg\min_{\mathbf{\mu}}\left[-L(\mathbf{y}\,|\,\mathbf{\mu}) + \lambda R(\mathbf{\mu})\right], \tag{1}$$

where $L(\mathbf{y}\,|\,\mathbf{\mu})$ is the log-likelihood function of the transmission measurements $\mathbf{y}$ given $\mathbf{\mu}$, and $R(\mathbf{\mu})$ is the regularizer. The positive parameter λ controls the balance between the likelihood and prior terms. The negative log-likelihood function is given by

$$-L(\mathbf{y}\,|\,\mathbf{\mu}) = \sum_i h_i([\mathbf{A}\mathbf{\mu}]_i),$$
$$\text{where } h_i(\mathbf{l}) = (b_i e^{-\mathbf{l}} + r_i) - y_i \log(b_i e^{-\mathbf{l}} + r_i). \tag{2}$$

In (2) y_i is the transmission measurement of the i-th ray, b_i is the blank scan counts of the i-th ray, and r_i is the mean of the background events. The term $[\mathbf{A}\mathbf{\mu}]_i = \sum_j a_{ij}\mu_j$ indicates the line

integral of the underlying object through the i-th ray, where the element a_{ij} of the system matrix $\mathbf{A}$ represents the contribution of the attenuation coefficient μ_j in the j-th pixel to the i-th ray.

To incorporate the WMP into the PL transmission reconstruction process, we basically follow the derivation of the median prior [9] originally developed for emission tomography, where an auxiliary field $\mathbf{m}$ in register with $\boldsymbol{\mu}$ is used so that the PL minimization problem becomes a joint minimization as follows: [9]

$$\hat{\boldsymbol{\mu}}, \hat{\mathbf{m}} = \arg\min_{\boldsymbol{\mu}, \mathbf{m}}\left[-L(\mathbf{y}\mid\boldsymbol{\mu}) + \lambda R(\boldsymbol{\mu}, \mathbf{m})\right]. \qquad (3)$$

In order to express the regularization term using the median operation with the aid of the auxiliary variable $\mathbf{m}$, we utilize a connection between an absolute value penalty and the median, such as $median\{\boldsymbol{\mu}\} = \arg\min_m \sum_j |\mu_j - m|$. [9] By modifying the absolute value function to a differentiable form, we define the following regularization term:

$$R(\boldsymbol{\mu}, \mathbf{m}) = \sum_j \sum_{j' \in N(j)} w_{jj'}\psi(\mu_j - m_{j'}), \text{where } \psi(\xi) = \sqrt{\xi^2 + \varepsilon}. \quad (4)$$

In (4) $N(j)$ represents a local neighborhood system of the j-th pixel including j-th pixel itself, ε is a positive parameter, which is small enough for the approximation to the absolute value $|\xi|$, and $w_{jj'}$ is the weight between j and j'. In this work, we consider a center-weighted median [4]-[8] whose weight $w_{jj'}$ is defined as

$$w_{jj'} = \begin{cases} 1, & j \neq j' \\ 2k-1, & j = j' \end{cases}, \text{where } k = 1, 2, \ldots, \frac{L+1}{2}. \qquad (5)$$

In (5) $L <$ (number of pixels in $N(j)$).

To solve the above joint minimization problem in (3), the following alternating iterative algorithm is used:

$$\hat{\boldsymbol{\mu}}^{n+1} = \arg\min_{\boldsymbol{\mu}}\left[-L(\mathbf{y}\mid\boldsymbol{\mu}) + \lambda^n R(\boldsymbol{\mu}, \hat{\mathbf{m}}^n)\right] = \arg\min_{\boldsymbol{\mu}} \Phi(\boldsymbol{\mu}, \hat{\mathbf{m}}^n). \qquad (6)$$

$$\hat{\mathbf{m}}^{n+1} = \arg\min_{\mathbf{m}}\left[R(\hat{\boldsymbol{\mu}}^{n+1}, \mathbf{m})\right]. \qquad (7)$$

In our previous work [3], to adaptively select the center weight w, we modeled w as a function of the roughness of neighbors derived from the point-wise standard deviation (SD) image of the previous estimate where the two-dimensional (2-D) SD image was transformed into a monotonically non-decreasing 1-D function constructed by the normalized cumulative histogram (NCH) of the SD image. A major advantage of using the NCH curve is that, unlike the method of manually constructing a series of pre-defined 1-D curves for iterative PL reconstruction, the NCH-based method updates the 1-D NCH curve at each iteration as soon as the new pixel μ_j is updated.

In this work, to adaptively select the smoothing parameter, we may use a similar approach to modeling the space-variant smoothing parameter λ_j as a function of the roughness of

neighbors. Note that, unlike the center weight of the median prior which increases the roughness as w is increased, the smoothing parameter decreases the roughness as λ is increased. Therefore, the function that determines λ_j must be monotonically non-increasing. To construct a 1-D monotonically non-increasing function at the n-th PL iteration using the NCH curve, we used the following formula:

$$\lambda_j^n = \lambda_{\max} - NCH(s_j^n), \qquad (8)$$

where λ_j^n is the smoothing parameter for the n-th iteration, $NCH(\cdot)$ is the NCH curve, $\lambda_{\max} = NCH(s_J^n)$ and $\mathbf{s}^n = \{s_j^n \mid j = 1, \ldots, J\}$ is a point-wise SD image that measures the pixel roughness. Note that, since $NCH(\cdot)$ is monotonically non-decreasing, λ_j^n gets smaller as s_j^n increases, and vice versa.

Optimization Method

In this work, we used the ordered-subsets separable paraboloidal surrogates (OS-SPS) algorithm [10] for the minimization on $\boldsymbol{\mu}$. For the minimization on $\mathbf{m}$, we used the Newton-Raphson method. In order to apply the OS principle [11] to the minimization on $\boldsymbol{\mu}$, the objective function in (6) can be decomposed into P angular subsets as follows: [11]-[13]

$$\Phi(\boldsymbol{\mu}, \hat{\mathbf{m}}^n) = \sum_{p=1}^{P} \Phi_p(\boldsymbol{\mu}, \hat{\mathbf{m}}^{n,p}),$$

$$\text{where } \Phi_p(\boldsymbol{\mu}, \hat{\mathbf{m}}^{n,p}) = \left\{\sum_{i \in S(p)} h_i([\mathbf{A}\boldsymbol{\mu}]_i)\right\} + \frac{\lambda^n}{P} R(\boldsymbol{\mu}, \hat{\mathbf{m}}^{n,p}). \qquad (9)$$

In (9) $S(p) \in \{S(p) \mid p = 1, \ldots, P\}$ is the p-th angular subset.

To solve the problem in (6) by the OS-SPS, the following separable quadratic surrogates are minimized in place of the decomposed objective function Φ_p at each iteration. [10], [13]

$$\phi_p(\boldsymbol{\mu}; \hat{\boldsymbol{\mu}}^n, \hat{\mathbf{m}}^{n,p}) = \Phi_p(\hat{\boldsymbol{\mu}}^n, \hat{\mathbf{m}}^{n,p}) + \nabla\Phi_p(\hat{\boldsymbol{\mu}}^n, \hat{\mathbf{m}}^{n,p})(\boldsymbol{\mu} - \hat{\boldsymbol{\mu}}^n)$$
$$+ \frac{1}{2}\breve{c}_{pj}(\hat{\boldsymbol{\mu}}^n, \hat{\mathbf{m}}^{n,p})(\boldsymbol{\mu} - \hat{\boldsymbol{\mu}}^n)^2 \geq \Phi_p(\boldsymbol{\mu}, \hat{\mathbf{m}}^{n,p}), \qquad (10)$$

where $\nabla\Phi_p$ denotes the first derivative of Φ_p and $\breve{c}_{pj}$ is the curvature of ϕ_p which is given by

$$\breve{c}_{pj}(\boldsymbol{\mu}, \hat{\mathbf{m}}^{n,p}) = \sum_{i \in S(p)} a_{ij}\gamma_i c_i([\mathbf{A}\boldsymbol{\mu}]_i) + \frac{2\lambda^n}{P}\sum_{j' \in N(j)} w_\psi(\mu_j - \hat{m}_{j'}^{n,p}), \qquad (11)$$

where $\gamma_i = \sum_j a_{ij}$. c_i and $w_\psi(\xi) = \nabla\psi(\xi)/\xi$ are the curvatures of the surrogates for the likelihood and the regularization terms, respectively. [14] In this work, we used the optimum curvature [13] for the surrogates for the likelihood term.

To estimate $\hat{\boldsymbol{\mu}}$ from the quadratic surrogate function in (10), the update equation for $\boldsymbol{\mu}$ is given by
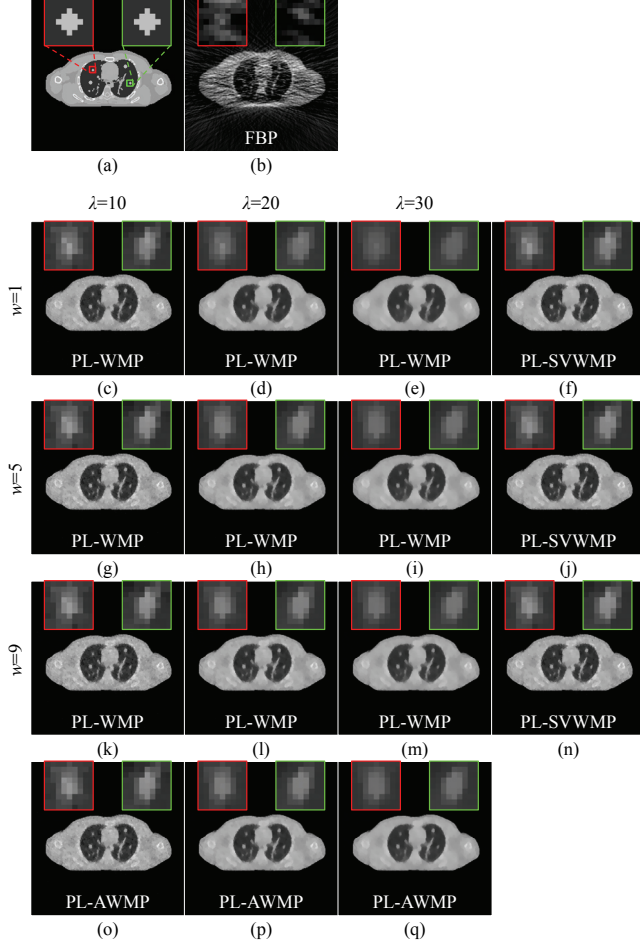
Figure 1. Phantom and anecdotal reconstructions: (a) phantom; (b) FBP; (c)-(q) PL (20 iterations of OS-SPS with 32 subsets); (c)-(f) w=1; (c) WMP (λ=10, PE=13.92%); (d) WMP (λ=20, PE=14.33%); (e) WMP (λ=30, PE=15.02%); (f) SVWMP (PE=13.80%); (g)-(j) w=5; (g) WMP (λ=10, PE=13.90%); (h) WMP (λ=20, PE=13.88%); (i) WMP (λ=30, PE=14.47%); (j) SVWMP (PE=13.62%); (k)-(n) w=9; (k) WMP (λ=10, PE=13.98%); (l) WMP (λ=20, PE=13.82%); (m) WMP (λ=30, PE=14.33%); (n) SVWMP (PE=13.61%); (o) AWMP (λ=10, PE=13.85%); (p) AWMP (λ=20, PE=13.87%); (q) AWMP (λ=30, PE=14.45%).

$$\hat{\mu}_j^{n,p+1} = \hat{\mu}_j^{n,p} - \frac{\sum_{i \in S(p)} a_{ij} \nabla h_i(l_i^{n,p}) + \frac{\lambda_j^n}{P} \sum_{j' \in N(j)} \nabla \psi(\hat{\mu}_j^{n,p} - \hat{m}_{j'}^{n,p})}{\sum_{i \in S(p)} a_{ij} \gamma_i c_i(l_i^{n,p}) + \frac{2\lambda_j^n}{P} \sum_{j' \in N(j)} w_\psi(\hat{\mu}_j^{n,p} - \hat{m}_{j'}^{n,p})}, \quad (12)$$

where $\hat{\mu}_j^{n,p}$ represents the j-th pixel value of $\mathbf{\mu}$ estimated from the p-th angular subset, and λ_j^n is obtained by using (8) at the n-th iteration.

Given $\hat{\mathbf{\mu}}^{n,p}$, the update equation for $\mathbf{m}$ is given by

$$\hat{m}_j^{n,p,k+1} = \hat{m}_j^{n,p,k}$$
$$+ \frac{\sum_j w_{jj'} \left(\hat{\mu}_j^{n,p} - \hat{m}_{j'}^{n,p,k} \right) \psi \left(\hat{\mu}_j^{n,p} - \hat{m}_{j'}^{n,p,k} \right)^{-1}}{\sum_j \varepsilon w_{jj'} \left[\left(\hat{\mu}_j^{n,p} - \hat{m}_{j'}^{n,p,k} \right)^2 + \varepsilon \right]^{-1} \psi \left(\hat{\mu}_j^{n,p} - \hat{m}_{j'}^{n,p,k} \right)^{-1}}. \quad (13)$$
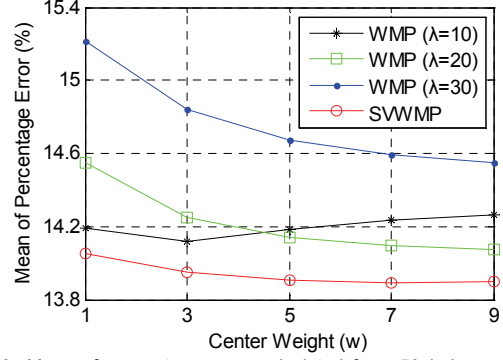
Figure 2. Mean of percentage error calculated from 50 independent noise trials for 5 different values of the center weight w.

Note that the final update value at the K-th iteration is assigned as $\hat{\mathbf{m}}^{n,p} = \hat{\mathbf{m}}^{n,p,K}$, where $\hat{\mathbf{m}}^{n,p}$ is the estimate at the end of the n-th iteration after processing K sub-iterations.

Experimental Results

For our simulation studies, the projection data were acquired from the 256×256 software phantom shown in Fig. 1(a) by using a fan-beam projector with 430 detector bins and 480 discrete angles over 360°. We tested with the following four reconstruction algorithms: filtered back-projection (FBP), PL with the WMP (PL-WMP), PL with the adaptive WMP (PL-AWMP) whose center weight is adaptively chosen by our previously developed method [3], and PL with the space-variant smoothing based WMP (PL-SVWMP) proposed in this work. Although our SVWMP method may be expandable to a space-variant smoothing based AWMP, we focus here only on PL-SVWMP method and show PL-AWMP for a comparison only.

Figure 1 (b) shows an FBP reconstruction and (c)-(q) show PL-WMP/AWMP/SVWMP reconstructions. For PL-WMP and PL-SVWMP, the center weight w was set to the three different values of 1, 5 and 9, and the smoothing parameter λ was set to the three different values of 10, 20, and 30. For PL-SVWMP, λ was adaptively chosen within the range of [10,30]. For PL-AWMP, the center weight was adaptively chosen, whereas the smoothing parameter was set to the three different values of 10, 20 and 30. Note that, for a given value of w, the PL-SVWMP method performs even better in terms of the percentage error (PE) than the PL-WMP method with the manually chosen λ for the best result. (Compare (c) with (f), (h) with (j), and (l) with (n).)

To test our proposed method more accurately, we performed 50 independent Poisson noise trials for each reconstruction method and measured the mean of percentage error (MPE) for each reconstruction method over 50 reconstructions for the five different values of w=1, 3, 5, 7 and 9, which is defined by

$$MPE = \frac{1}{K} \sum_{k=1}^{K} PE^k,$$
$$\text{where } PE^k = \sqrt{\sum_j \left(\mu_j - \hat{\mu}_j^k \right)^2 / \mu_j^2} \times 100\%. \quad (14)$$

In (14) K=50 is the total number of independent noise trials, μ_j is the pixel located at j in the phantom and $\hat{\mu}_j^k$ is the pixel located at

(a)

(b)

(c)

(d)

(e)
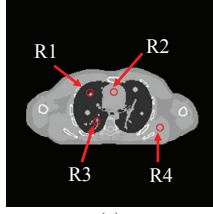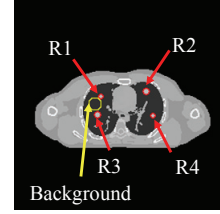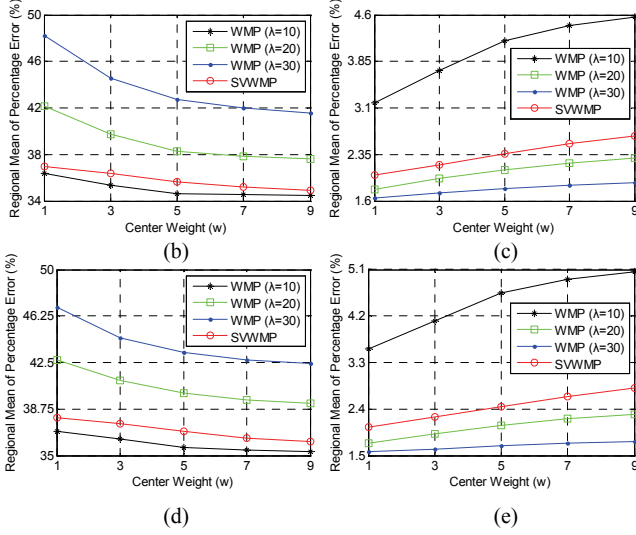
Figure 3. Regional mean of percentage error calculated from 50 independent noise trials for 5 different values of the center weight w: (a) ROIs for regional MPE; (b) R1; (c) R2; (d) R3; (e) R4.

(a)

(b)

(c)

(d)

(e)

Figure 4. Regional contrast recovery coefficient (CRC) versus background standard deviation: (a) ROIs for regional CRC; (b) R1; (c) R2; (d) R3; (e) R4.

j in the k-th reconstruction. Figure 2 shows that, for a relatively large smoothing parameter, as the center weight w is increased, the MPE is decreased. However, it is important to point out that the SVWMP method is less sensitive to the variation of the center weight than the standard WMP shown in Fig., which indicates that the SVWMP method controls the smoothing parameter efficiently. Note that the WMP method with $\lambda=10$ is exceptional in that it does not follow the characteristic of other WMP methods. This is presumably due to the fact that the value of 10 for the smoothing parameter is small enough to increase the PE for the weight w greater than 3.

To evaluate the quantitative performance of our proposed method, we measured the regional MPE for each region of interest (ROI) shown in Fig. 3(a), which is defined by

$$MPE_{\mathfrak{R}} = \frac{1}{K} \sum_{k=1}^{K} PE_{\mathfrak{R}}^{k},$$

$$\text{where } PE_{\mathfrak{R}}^{k} = \sqrt{\sum_{j \in \mathfrak{R}} \left(\mu_j - \hat{\mu}_j^k \right)^2 \Big/ \mu_j^2} \times 100\%. \tag{15}$$

Figure 3(b)-(e) show center weight versus MPE curves for PL-WMP with three different values (10, 20, 30) of λ and PL-SVWMP. For the regions (R1 and R3) containing edges, the MPEs decrease as λ is increased. On the other hand, for the monotonic regions (R2 and R4), the MPEs increase as λ is increased. Note that, while the PL-WMP with $\lambda=10$ yields minimal MPEs in R1 and R3 over the range of the center weight, it performs worst in R2 and R4,

which indicates that the PL-WMP has a limitation in restoring monotonic regions. In contrast the PL-SVWMP performs equally well in all regions.

We also measured the regional contrast recovery coefficients (CRCs) for the pre-selected ROIs shown in Fig. 4 (a). The CRC in each ROI is defined as

$$CRC_{\mathfrak{R}}^{k} = \frac{CR_{\mathfrak{R}}^{k}}{CR_{\mathfrak{R}}^{0}}, \text{where } CR_{\mathfrak{R}}^{k} = \frac{\left| Z_{\mathfrak{R}}^{k} - Z_{B}^{k} \right|}{Z_{B}^{k}}. \tag{16}$$

In (16), $CR_{\mathfrak{R}}^{0}$ is the true contrast in the phantom, Z_{B}^{k} is the mean attenuation in the background region, and $Z_{\mathfrak{R}}^{k} = \sum_{j \in \mathfrak{R}} \hat{\mu}_j^k / m_{\mathfrak{R}}$, where $Z_{\mathfrak{R}}^{k}$ represents the mean attenuation in each ROI $\mathfrak{R}$ at the k-th noise trial and $m_{\mathfrak{R}}$ is the number of pixels in each ROI $\mathfrak{R}$. The ensemble mean of CRC is defined as

$$\overline{CRC}_{\mathfrak{R}} = \frac{1}{K} \sum_{k=1}^{K} CRC_{\mathfrak{R}}^{k}. \tag{17}$$

While the CRC represents the degree of the recovered contrast of a region relative to the background region, it does not show how much the background noise is involved. In order to overcome this limitation, we measured the SD of the background noise as follows:

$$\bar{\sigma} = \frac{1}{K}\sum_{k=1}^{K}\sigma^k,$$

$$\text{where } \sigma^k = \sqrt{\frac{1}{m_B-1}\sum_{j\in B}\left[\hat{\mu}_j^k - \left(\frac{1}{m_B}\sum_{j'\in B}\hat{\mu}_{j'}^k\right)\right]^2}. \qquad (18)$$

In (18) m_B is the number of pixels in background region B. Figure 4(b)-(e) show the CRC versus SD curves for PL-WMP reconstructions with the three different values (10, 20, 30) of λ and for PL-SVWMP, where each point indicates the center weight w set to 1, 3, 5, 7 and 9. Note that the WMP method reveals a large variation of SD by changing the value of the smoothing parameter from 10 to 30. While the WMP method with λ=20 or 30 reveals small SD, the WMP method with λ=10 suffers from significantly high SD. On the other hand, the SVWMP method not only reveals high CRCs almost comparable to the WMP method with λ=10, but also maintains low SD.

Conclusion

We have developed a space-variant smoothing based PL-WMP method for transmission tomography reconstruction. This work improves our previous work for the PL-WMP method [3] by alleviating the problem of adjusting the smoothing parameter that weights the prior (or regularizer) term with respect to the likelihood term. Since our method uses a histogram of the SD image obtained from the previous estimate $\hat{\boldsymbol{\mu}}^{n-1}$ that is very close to the current estimate $\hat{\boldsymbol{\mu}}^n$, it provides important information about the roughness of neighbors of a pixel at each iteration.

Therefore, as compared to our previous work, where the smoothing parameter was manually chosen and fixed for all iterations, our new SVWMP method adaptively changes the selected smoothing parameter at each pixel location for each iteration, thereby efficiently improving the reconstruction accuracy.

Acknowledgments

References

[1] J. Hsieh, B. Nett, Z. Yu, K. Sauer, J.-B. Thibault, and C. A. Bouman, "Recent advances in CT image reconstruction," Current Radiology Reports, vol. 1, no. 1, pp. 39-51, 2013.

[2] J. E. Jung, and S.-J. Lee, "Edge-preserving iterative reconstruction for transmission tomography using convex weighted median priors," Conf. Rec. IEEE Nucl. Sci. Sym. & Med. Imag. Conf., 2015.

[3] J. E. Jung and S.-J. Lee, "An adaptive method for weighted median priors in transmission tomography reconstruction," Proc. of SPIE Medical Imaging, vol. 9783, pp. 97834P1-P8, 2016.

[4] D. R. K. Brownrigg, "Weighted median filters," Commun. Assoc. Comput. Machinery, vol. 27, no. 8, pp. 807–818, 1984.

[5] S. J. Ko and Y. H. Lee, "Center weighted median filters and their applications to image enhancement," IEEE Trans. Circuits Systems, vol. 38, no. 9, pp. 984–993, 1991.

[6] T. Song, M. Gabbouj, and Y. Neuvo, "Center weighted median filters: Some properties and applications in image processing," Signal Processing, vol. 35, no. 3, pp. 213–229, 1994.

[7] L. Yin, R. Yang, M. Gabbouj, and Y. Neuvo, "Weighted median filters: a tutorial, " IEEE Trans. Circuits and Systems II: Analog and Digtal Signal Processing, vol. 43, pp. 3, pp. 157-192, 1996.

[8] T. Chen and H. R. Wu, "Adaptive impulse detection using center-weighted median filters," IEEE Signal Processing Letters, vol. 8, no. 1, pp. 1-3, 2001.

[9] I.-T. Hsiao, A. Rangarajan and G. Gindi, "A new convex edge-preserving median prior with applications to tomography," IEEE Trans. Med. Imag., vol. 22, no. 5, pp. 580-585, 2003.

[10] H. Erdoğan and J. A. Fessler, "Ordered subsets algorithms for transmission tomography," Phys. Med. Biol., vol. 44, no. 11, pp. 2835-2851,1999.

[11] H. M. Hudson and R. S. Larkin, "Accelerated image reconstruction using ordered subsets of projection data" IEEE Trans. Med. Imag., vol 13, no. 4, pp. 601–609, 1994.

[12] V. M. Kibardin, "Decomposition into functions in the minimization problem," Automat. Remote Control, vol. 40, pp. 1311–1323, 1980.

[13] S. Ahn, J. A. Fessler, D. Blatt, and A. O. Hero, "Convergent incremental optimization transfer algorithms: application to tomography," IEEE Trans. Med. Imag., vol. 25, no. 3, pp. 283-296, 2006.

[14] H. Erdoğan and J. A. Fessler, "Monotonic algorithms for transmission tomography," IEEE Trans. Med. Imag., vol. 18, no. 9, pp. 801–814, 1999.

Author Biography

Ji Eun Jung received her B.S. and M.S. degrees in Electronic Engineering from Paichai University of Korea in 2013 and 2015, respectively. She is currently enrolled in the Double Degree Program for Ph.D. in Electronic Engineering at Paichai University in Korea and Computer Science and Electrical Engineering at Kumamoto University in Japan. Her research interests include image processing and medical imaging. In particular, she is interested in image reconstruction for emission and transmission tomography.